Hindawi
International Journal of Electrochemistry
Volume 2018, Article ID 1273768, 15 pages
https://doi.org/10.1155/2018/1273768

Research Article

The Redox Chemistry of Ruthenium Dioxide: A Cyclic Voltammetry Study—Review and Revision

Sebastian Chalupczok, Peter Kurzweil, Helmut Hartmann, and Christian Schell

University of Applied Sciences, Kaiser-Wilhelm-Ring 23, 92224 Amberg, Germany

Correspondence should be addressed to Peter Kurzweil; p.kurzweil@oth-aw.de

Received 30 August 2017; Revised 14 December 2017; Accepted 20 December 2017; Published 1 February 2018

Academic Editor: Gerd-Uwe Flechsig

By cyclic voltammetry at high scan rates, the electrochemical properties of RuO_2 in acidic and alkaline solutions were investigated in detail. Thirteen current peaks can be distinguished in sulfuric acid and sodium hydroxide. With respect to the pH sensitivity of RuO_2 electrodes, we considered charge calculations, peak currents, and apparent diffusion coefficients. The nature of the Ru(II) oxidation was clarified by Ru(I)–Ru(III) species.

1. Introduction

The redox activity of platinum metal oxides has been considered for electrolysis, electrochemical storage devices, and pH sensors [1–4]. Ruthenium dioxide electrodes have been studied since the early 1970s because of the mixed electronic and ionic conductivity ($35.2 \pm 0.5\,\mu\Omega\cdot$cm) [5]. Despite many attempts, the mechanisms of the electrochemical processes on a RuO_2 electrode in acidic and alkaline solutions, as well as in organic solvents, are not fully understood. Since the RuO_2/solution interface behaves like an electric capacitor, that can be charged and discharged very quickly, we employ cyclic voltammetry [6, 7] for in-depth analysis of the redox processes in the electrode surface.

This paper considers the electrochemical behavior of thermally produced RuO_2 electrodes in acidic and alkaline solutions with special respect to the oxygen (OER) and hydrogen evolution reactions (HER) in different solutions.

2. Experimental

2.1. Preparation of Electrodes. Electrodes were prepared by thermal decomposition of commercial-grade ruthenium(III) chloride hydrate (Sigma-Aldrich) on titanium supports (thermal spray pyrolysis).

$$2\left(RuCl_3 \cdot 3H_2O\right) + \frac{1}{2}O_2 \rightleftharpoons 2\left(RuO_2 \cdot 1.5H_2O\right) + 6HCl \quad (1)$$

The oxide formation takes place at a temperature of about 360°C [8], which was verified by thermogravimetric analysis using a Netzsch 209 F1 Libra (TGA) in a platinum-rhodium crucible under oxygen atmosphere (Figure 1). The mass change is determined by the evaporation of both adsorbed water and crystal water and the formation of the oxide phase.

To ensure good adhesion on titanium (thickness 0.050 mm, Ankuro Int. GmbH), the substrate was roughened and degreased with acetone. Then a slurry of $RuCl_3 \cdot xH_2O$ in acetone was applied to the substrate which was clamped in a coating frame with sealed recesses. After drying overnight, the heat treatment was carried out in a furnace in air at 500°C for 2 h. The mass of the resulting $d = 2\,\mu$m thick RuO_2 layer was $m/A = 8.0\,\text{mg cm}^{-2}$ (electrode area: $1\,\text{cm}^2$). According to $\varrho d = m/A$, the calculated density equals $\varrho = 4\,\text{g cm}^{-3}$, which suggests a porosity of 57% with respect to the theoretical density of compact RuO_2 ($7\,\text{g cm}^{-3}$). Zinc ion adsorption measurements of Savinell et al. [9] suggest $14.6 \pm 1.6\,\text{cm}^2\,\text{mg}^{-1}$ (Ti|RuO_2, annealed at 450°C for 1 h). Hence, the electrochemically active surface amounts to 100–120 cm^2. Impedance spectra confirm a capacitance of about 4 mF cm^{-2}

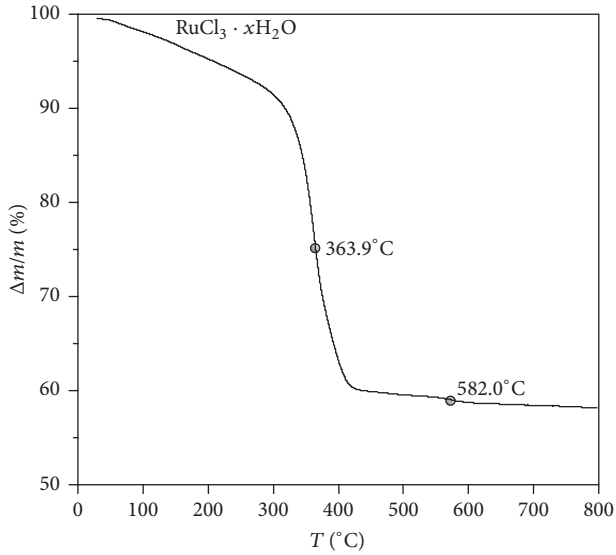

Figure 1: Thermogravimetric analysis of ruthenium chloride.

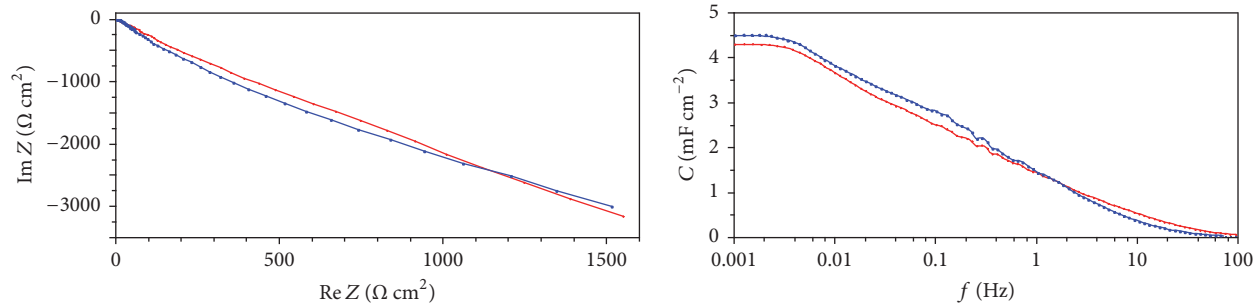

Figure 2: Complex plane plot of impedance and frequency response of capacitance of a cell of two identical RuO_2/Ti electrodes in 1-molar sulfuric acid (red) and 1-molar sodium hydroxide solution (blue). Capacitance calculated for single electrode, $C(\omega) = 0.5 \cdot [-\omega \operatorname{Im} \underline{Z}(\omega)]^{-1}$.

(0.4 F per real cm^2) in aqueous solution (Figure 2). The BET surface of thermal RuO_2 powders (roughly 100 $m^2 g^{-1}$) drops with heat treatment to less than 10 $m^2 g^{-1}$ due to sintering of the particles.

2.2. Instruments and Methods. Cyclic voltammetry was carried out with a three-electrode arrangement using a potentiostat/galvanostat (EC301, Stanford Research Systems, Inc.). A reversible hydrogen electrode (RHE) was used as the reference electrode, and a platinum sheet (12 cm^2) as the counterelectrode. All measurements employed 1 M H_2SO_4 or 1 M NaOH at a constant temperature of 25 ± 0.5°C. The RuO_2 powder was characterized by X-ray diffraction (XRD, Rigaku Miniflex 600) and SEM/EDX (Stereoscan LEO 440).

3. Results and Discussion

3.1. Characterization of Electrodes. Figure 3 compiles the X-ray diffractograms of RuO_2, prepared by thermal decomposition of $RuCl_3 \cdot xH_2O$ at different temperatures. As confirmation of the thermogravimetric analysis, the generation of the

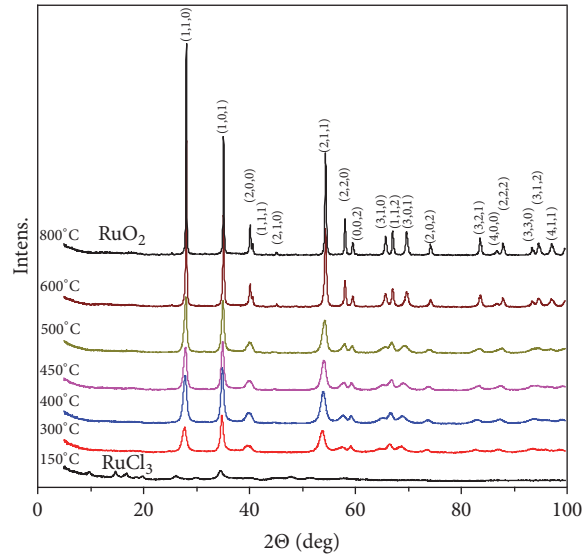

Figure 3: XRD measurements of the thermally decomposed $RuCl_3$ hydrate to RuO_2 by annealing with different temperatures.

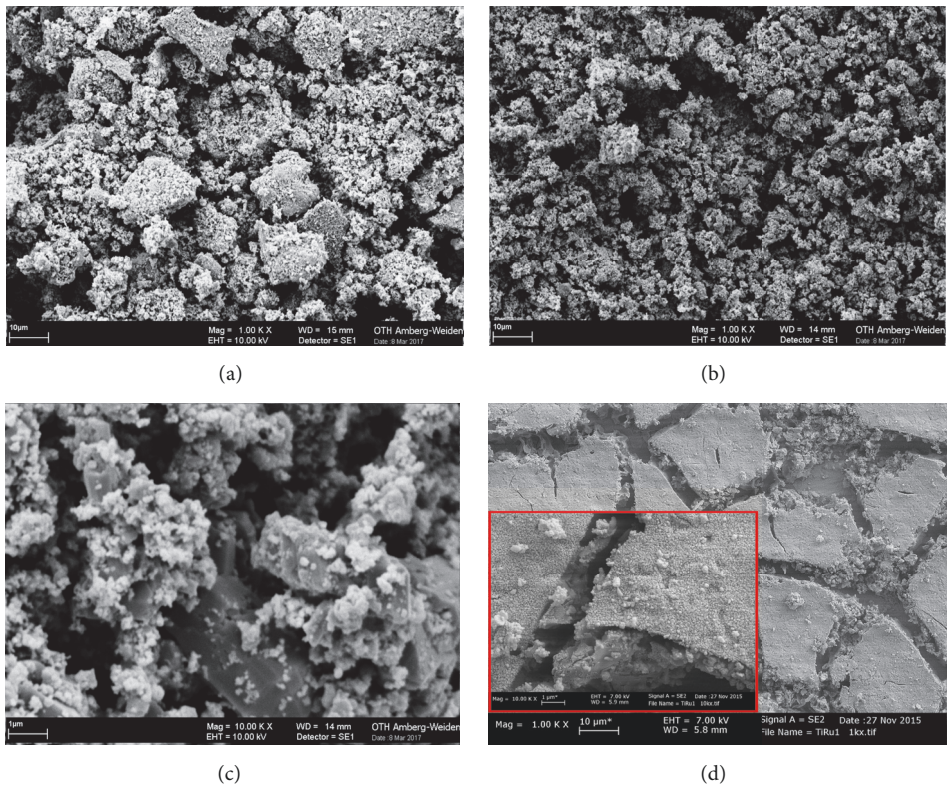

Figure 4: SEM images of RuO_2 prepared at (a) 300°C, 1000-fold magnification, (b) 600°C, 1000x, (c) 600°C, 10000x; (d) RuO_2 coated on titanium by thermal spray pyrolysis at 500°C (1000x), insert at 10000-fold magnification.

oxide is obvious to take place at temperatures between 300°C and 400°C.

Below 300°C, amorphous $RuO_2 \cdot xH_2O$ is received, which contains a residual chloride. The diffraction peaks at $2\Theta < 28^\circ$ were attributed to chloride. Above 300°C, the rutile structure of crystalline RuO_2 appears more and more; the crystal system is tetragonal.

The main peak at about $2\Theta = 28^\circ$ belongs to (110), and (101) occurs at $2\Theta = 35^\circ$. With rising temperature, the full width at half maximum (FWHM) drops as the diffraction peaks become sharper. Additionally, further lattice planes are formed. According to the Debye-Scherrer equation, the average size of the crystallites was calculated:

$$d = \frac{K\lambda}{\mathrm{FWHM}\,(2\Theta) \cdot \cos\,(\Theta)}, \quad (2)$$

wherein d is the particle size in nm, λ is the X-ray wavelength (Å or pm), K is a shape factor, and Θ is the Bragg angle. At 500°C, the calculated particle size is approximately 14.7 nm (110) and 15.6 nm (101), respectively. The lattice constants at 500°C read the following: $a = b = 450.4$ pm and $c = 311.5$ pm.

Most of the ruthenium and oxygen atoms in the bulk material are present in the crystal orientations (110) and (101), whereas (101), (111), and (100) exist predominantly on the material surface [10]. Hence, the electrochemical properties of polycrystalline RuO_2 are determined by the (110) face.

The rutile structure of stoichiometric RuO_2 (110) [11] consists of a slightly distorted octahedron with 4 equatorial and 2 apical Ru-O directions. On the surface, bridging oxygen atoms are coordinated with two Ru atoms underneath, and a Ru atom on a onefold coordinatively unsaturated site is coordinated with five oxygen atoms [12].

The SEM/EDX measurements (Figure 4) show the microporous powder morphology of RuO_2 and the unavoidable content of chlorine (about 5%) that is caused by thermolysis of the $RuCl_3$ precursor. Our previous TOF-SIMS study [13] showed residual chlorine bound in Ru-O-Cl clusters. Although the EDX analysis gives only a rough estimate of the surface, because of the limited penetration depth of the X-rays, some surplus of oxygen beyond the formula RuO_2 was observed. This is partly due to adsorbed and bound water, especially as some three-valent ruthenium is present at the surface in compositions up to $Ru(OH)_3$.

The RuO_2 layer reveals an undesired particle agglomeration due to the thermal treatment at 600°C. In contrast to that, the 300°C powder exhibits particle sizes of approximately 17.8 ± 2.9 μm, and a porous structure around an average pore size of 1.4 ± 0.5 μm. At 600°C the particle size is about 8.6 ± 2.3 μm, and the pore widths decrease to 0.87 ± 0.3 μm. In particular, some small particles of the size 0.75 ± 0.4 μm adhere forming agglomerates.

Over et al. [14] showed that an ultrathin RuO_2 (110) film can be formed on ruthenium exposed to oxygen. Once a

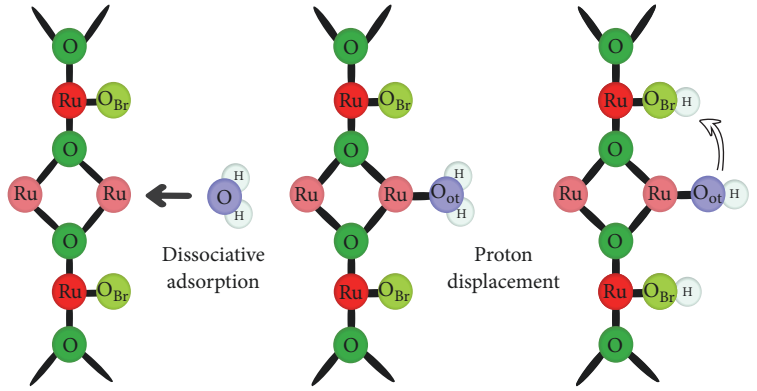

FIGURE 5: Mechanism of the dissociative adsorption of water and proton displacement during anodic charging of RuO_2 (this work based on [1, 4, 10, 12]).

nucleus has formed, it grows autocatalytically forming large domains of RuO_2 (110). Oxide growth is limited by the mass transport of oxygen and metal ions across the oxide film.

Furthermore, ruthenium is able to incorporate dissolved oxygen into the basal plane [15, 16]. In the SEM image (Figure 4(d)), RuO_2 coated on titanium shows a fissured surface around sponge-like areas of approximately 43 ± 14 μm. The pimpled nanostructure is made up of particle sizes of 0.1 ± 0.03 μm, and the vacancies between these particles are approximately 0.03 ± 0.01 μm. The cracks, caused by the evaporation of the solvent, are about 4.6 ± 1.0 μm wide. The inserted magnification shows the bright nanoparticles (0.61 ± 0.4 μm) described above. The above results confirm the extraordinarily porous structure of thermally prepared RuO_2.

3.2. Mechanism of Water Adsorption. The RuO_2 surface is covered by a carpet of OH groups due to the dissociative adsorption of water followed by proton displacement [1]. Bridged oxygen is seldom the preferred adsorption site for most molecules, but it is relevant to hydrogen adsorption which results in OH groups with bridged O atoms [12]. Two sorts of hydroxyl groups are formed during anodic charging: $O_{Br}H$ with bridged oxygen and $O_{ot}H$, which exists only on onefold coordinatively unsaturated Ru atoms; see Figure 5. The Ru atom acts as a Lewis acid/base (electron acceptor), whereas O_{Br} is a Brønsted base (proton acceptor).

Due to the dissociative adsorption of water, protons (or hydroxide sites) from the surrounding electrolyte can penetrate into the porous electrode. The proton exchange between RuO_2 surface and aqueous solution reads as follows [1]:

$$RuO_x(OH)_y + ze^- + zH^+ \rightleftharpoons RuO_{x-z}(OH)_{y+z} \quad (3)$$

$$\text{Simplified: } Ru^{IV}O_2 + e^- + H^+ \rightleftharpoons Ru^{III}O(OH) \quad (4)$$

According to Nernst's equation the redox potential of the RuO_2 electrode depends on the pH value:

$$E = E^0 - \frac{RT}{F}\ln\frac{c\left(Ru^{III}\right)}{c\left(Ru^{IV}\right)\cdot c\left(H^+\right)} = E^0 - \frac{\ln 10\cdot RT}{F}\left(pH + \log\frac{c\left(Ru^{III}\right)}{c\left(Ru^{IV}\right)}\right) \quad (5)$$

$$(25^\circ C) \quad E = E^0 - 0.059\,V\cdot pH, \quad (6)$$

whereby the thermodynamically calculated standard potential (versus the SHE) equals $E^0 = 0.94$ V [17].

3.3. Electrochemistry in Acidic Solution. The cyclic voltammograms at rates up to 4000 mV/s reveal more than ten different peaks; see Figure 6. The open circuit potential (OCP) of RuO_2 in 1-molar H_2SO_4 was 0.92 V, in good agreement with the calculated standard potential and results of other authors (range 0.90–0.95 V) [3]. At the OCP, there is an equilibrium of Ru(IV) and Ru(III). The region 0–0.4 V can be attributed to the hydrogen sorption, which is also known from platinum [18]. As well, at RuO_2 single crystals, Hepel and coworkers [10] attributed the two peaks at 0 V and 0.24 V in 0.5 M H_2SO_4 to the hydrogen adsorption on the surfaces (110) and (001). The cathodic reduction of RuO_2 to metallic ruthenium does not occur during cyclic voltammetry, in contrast to the platinum electrode. This was verified by SEM/EDX results which do not show any metallic ruthenium on the support.

According to the mechanism in Figure 5, the anodic peak 1 at about 26 ± 15 mV in 1 M H_2SO_4 reflects the hydrogen adsorption on the onefold coordinatively unsaturated Ru atom.

If oxygen is present, which is the case for (110) surfaces, the second peak 2 at 143 ± 9 mV is most likely due to the hydrogen adsorption at oxygen. Hepel and coworkers [10] describe the hydrogen oxidation peaks as follows:

$$\text{Peak 1: } H_3O^+ + \overline{Ru} + e^- \rightleftharpoons \overline{Ru}\cdot H + H_2O \quad (7)$$

$$\text{Peak 2: } H_3O^+ + \overline{O} + e^- \rightleftharpoons \overline{O}\cdot H + H_2O \quad (8)$$

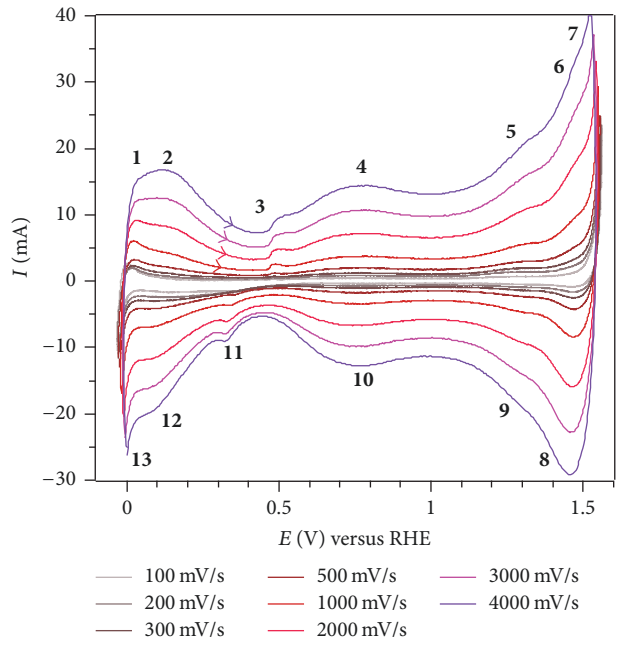

FIGURE 6: Cyclic voltammograms of a Ti/RuO_2 electrode in 1-molar H_2SO_4 (pH 0.08) at 25°C at different scan rates; 2nd cycle. Counterelectrode: platinum sheet. The electrolyte resistance (R_e = 1.8 Ω) was corrected. Arrows: oxidation wave in anodic direction. Reference electrode: reversible hydrogen electrode: V RHE = V SHE − 0.059 pH.

The reduction peak 12 at 75 ± 24 mV (and a previous shoulder at 247 ± 13 mV) reflects the hydrogen sorption at RuO_2 that can already be seen at moderate scan rates of 100–200 mV/s and includes chemical and electrochemical steps. Peak 3 at about 490 ± 12 mV either may be due to the preparation of the electrode and is typical for measurements in concentrated solutions; if the 1-molar sulfuric acid is diluted to 0.1 molar, the peak disappears. The reduction peak 11 corresponds at about 333 ± 14 mV. Doblhofer et al. [3] speculated that Ru(II) might be present in the hydrogen region. We suggest that Ru(II) might be a mixed Ru(I)–Ru(III) species in a cluster ion. The assumption of Ru(III) at 400 mV is in good agreement with thermodynamic data that the conversion of Ru(III) to Ru(IV) takes place within 0.4–1.0 V. That supports the theory that any unstable oxide, only stable in highly conductive acids, might be formed in the course of the rearrangement of surface oxides. Peak 4 reflects the Ru(III)/Ru(IV) redox couple at about 756 ± 11 mV and the reduction peak 10 at about 744 ± 16 mV. Michell et al. [19] confirm 780 mV, and 750 mV was found by Doblhofer et al.

$$\text{Peak } \underline{4}\text{: } 2RuO_2 + 2H^+ + 2e^- \rightleftharpoons Ru_2O_3 + H_2O \qquad (9)$$

Modified notations of (9) consider that Ru(III) can be written as $2Ru(OH)_3 \equiv Ru_2O_3 \cdot 3H_2O \equiv 2RuO(OH) + 2H_2O$, which leads back to (4). Anyway, the number of exchanged protons per ruthenium atom equals $z = 1$. The interesting fact is the pH dependence of the equilibrium potential that can be used for a potentiometric pH sensor [1]. A screen printed RuO_2 electrode on polyester film (versus a saturated calomel reference) reveals a sensitivity of −51.2 mV/pH (pH 2–9), but unfortunately it shows a potential drift due to continuous corrosion [20].

A screen printed RuO_2/Ta_2O_5 electrode (70 : 30 wt%) achieved −56 mV/pH versus Ag|AgCl (pH 2–12). So far, all pH sensors based on metal oxides suffer from hysteresis effects and interferences [21].

Galizzioli et al. [22] concluded that roughly 6-7% of the RuO_2 particles are able to participate in the reaction and pointed to the oxygen deficiency stoichiometry of the oxide. High annealing temperatures and oxygen atmosphere lead to less Ru(III), and the amorphous regions give way to crystalline oxide.

Peak 5 at 1286 ± 15 mV follows the continuous oxidation of the RuO_2 and might be attributed either (i) to a transition state followed by further oxidation to Ru(V) [3] or (ii) to Ru(VI) as suggested by Burke et al. [23–25]. Whereas Ru(V) is considered to be instable, the existence of Ru(VI) was proved by XPS studies, RuO_2 prepared by $RuCl_3$ thermolysis. Ru(VI) should be stable during anodic polarization in 1 M H_2SO_4 [26]. Recent thermodynamic calculations for ruthenium in aqueous solutions at different pH postulate solid ruthenium(V) oxide [27], having the standard electrode potential $E^0 = 1.222$ V (at $1.94 < \text{pH} < 2.55$). This is in excellent agreement with our peak at 1286 ± 15 mV, corrected by one pH step. The corresponding reduction peak 9 occurs at 1284 ± 19 mV.

$$\text{Peak } \underline{5}\text{: } \frac{1}{2}Ru_2O_{5(s)} + 3H^+ + e^- \rightleftharpoons Ru(OH)_2{}^{2+} + \frac{1}{2}H_2O \qquad (10)$$

Peak 6 at about 1441 ± 4 mV and its reduction 8 at 1463 ± 4 mV in acidic solution correspond to thermodynamic

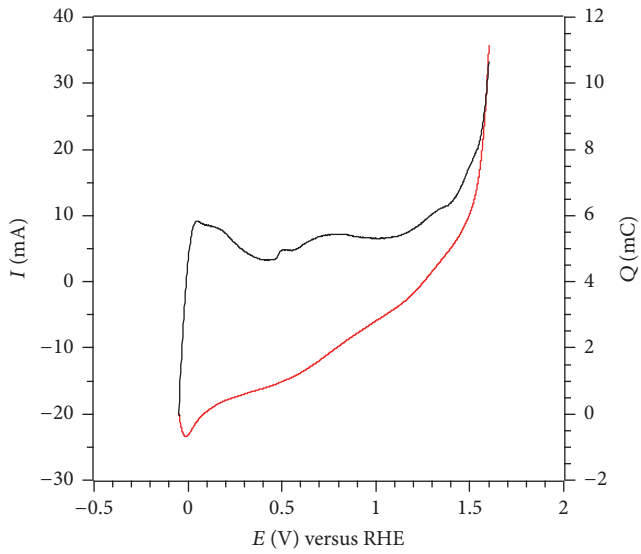

Figure 7: Anodic potential sweep and electric charge (red) of a RuO_2/Ti electrode at 2000 mV/s in 1 M H_2SO_4 (25°C).

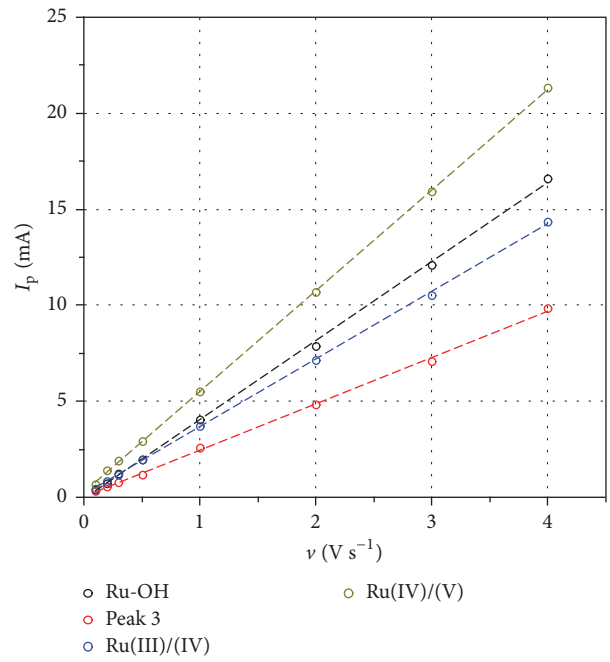

Figure 8: Changes of peak current with the applied scan rate of a RuO_2/Ti electrode in 1-molar H_2SO_4 (25°C). Fit quality: Ru-OH (R^2 = 0.9994); Peak 3 (R^2 = 0.9992); Ru(III)/(IV) (R^2 = 0.9996); Ru(IV)/(V) (R^2 = 0.9999).

calculations of Ru(VIII) in the range 1.94 < pH < 5.94 at a standard the potential E^0 = 1.466 V [27].

$$\text{Peak } \underline{6}\text{: } H_2RuO_5 + 3H^+ + 3e^- \rightleftharpoons \frac{1}{2}Ru_2O_{5(s)} + \frac{5}{2}H_2O \quad (11)$$

Further oxidation (>1.4 V RHE) results in the dissolution of ruthenium oxide as $H_2RuO_5 \rightarrow RuO_4 + H_2O$, which is a known corrosion product during violent electrolytic oxygen evolution [28, 29]. At Peak $\underline{7}$ (about 1.6 V) the oxygen evolution reactions start.

3.3.1. Electrochemical Valency. In order to distinguish between reversible and irreversible electron transfer, the redox peaks were evaluated with respect to peak current, potential, and electric charge. According to the theory of cyclic voltammetry, the potential difference is about 59 mV between the oxidation peak and the reduction peak of a totally reversible electron transfer. The peak currents for a reversible electron transfer should be identical.

$$\Delta E_p = \frac{59}{z}\,\text{mV}, \qquad \frac{i_p^a}{i_p^c} = 1. \quad (12)$$

Table 1 compiles the calculated number of exchanged electrons z of the redox process. Because of overlapping peaks it was sometimes difficult to identify the correct peak potentials. Electric charge was determined by numerical integration of the anodic branch of the cyclic voltammogram (see Figure 7). The charge needed for the Ru(III) → Ru(IV) transition was 2014 μC/cm^2 (0.5–1.0 V, geometric electrode area 1 cm^2, roughly 0.24 C per real cm^2) at 100 mV/s. This value is confirmed by Doblhofer et al. who assumed 1750 μC/cm^2 for one-electron change of the surface atoms [3].

Peak $\underline{1}$ associated with the hydrogen oxidation seems to be a reaction with poorly reversible electron passage, according to the peak current ratio between 0.76 and 0.81.

The potential of Peak $\underline{2}$ could not be evaluated correctly because of the overlap with Peak $\underline{1}$. The calculated charge between 0.055 V and 0.4 V results in a possible reaction that requires one electron. Doblhofer et al. suggested the redox reaction Ru(II) → Ru(III) for this step.

A reversible electron transfer can be postulated for Peaks $\underline{4}$, $\underline{5}$, and $\underline{6}$. The generation of Ru(IV) from Ru(III) according to (9) needs one electron per Ru atom. This is approximately confirmed by both the peak potential difference and the calculated charge.

The further oxidation to Ru(V) at Peak $\underline{5}$, related to (10), involves a one-electron transfer. The higher the potential is, the more the electrons are consumed by the oxygen evolution and oxidation of the electrode surface. Therefore, the electrons calculated vary with the two methods. Equation (11) suggests three electrons for the Ru(V) → Ru(VIII) oxidation. This is confirmed by the peak potential method, but the calculated electrons from the charge propose a one-electron transfer reaction Ru(VII) → Ru(VIII) [24, 25].

$$RuO_4^- \rightleftharpoons RuO_4 + e^- \quad (13)$$

No matter what reaction takes part, the peak current ratios of Peaks $\underline{6}$ and $\underline{8}$ indicate a reversible electron transfer. Figure 8 shows the peak currents plotted against scan rates.

Table 1: Calculated electrons for each redox reaction using peak potential differences and calculated charge with different scan rates in 1 M H_2SO_4. The errors ΔE and ΔQ relate to the accuracy of the potential and charge measurements. $z \approx 1$ denotes perfect one-electron redox reaction, $z \ll 1$ redox reaction along with sorption. The estimated approximate value is the weighted average of both methods without outliers (in parentheses).

Peak	1: Ru-H			2: Ru-OH			3			4: $Ru_2(III)O_3/2Ru(IV)O_2$			5: Ru(IV)/Ru(V)			6: Ru(V) → Ru(VIII)		
mV/s	$z(\Delta E_p)$	$z(Q)$	$i_p{}^a/i_p{}^c$	$z(\Delta E_p)$	$z(Q)$	$i_p{}^a/i_p{}^c$	$z(\Delta E_p)$	$z(Q)$	$i_p{}^a/i_p{}^c$	$z(\Delta E_p)$	$z(Q)$	$i_p{}^a/i_p{}^c$	$z(\Delta E_p)$	$z(Q)$	$i_p{}^a/i_p{}^c$	$z(\Delta E_p)$	$z(Q)$	$i_p{}^a/i_p{}^c$
100	(4.4)	(1.2)	1.6	(0.3)	(1.2)	0.2	0.1	0.1	–	(0.7)	2.0	1.2	1.2	1.4	1.3	(26)	0.9	1.3
200	0.8	0.7	0.8	(3.7)	0.8	0.3	0.1	0.1	–	(2.9)	1.9	1.9	(3.7)	(1.6)	1.5	3.9	1.2	1.3
300	1.0	0.5	0.8	–	0.9	–	0.4	0.1	0.5	1.6	1.8	1.1	(2.6)	(1.6)	1.4	(6.5)	1.2	1.2
500	1.0	0.3	0.8	–	1.0	–	0.4	0.1	0.6	2.0	1.8	1.2	(9.0)	1.4	1.2	(15)	1.3	1.1
1000	1.0	0.4	0.9	–	1.0	–	0.4	0.2	0.7	0.8	1.7	1.1	(5.0)	1.3	1.2	(4.5)	1.2	1.1
2000	1.1	0.3	0.8	–	0.9	–	0.3	0.2	0.8	1.0	1.7	1.1	(2.6)	1.4	1.2	3.5	1.1	1.1
3000	1.3	0.4	0.8	–	0.9	–	0.3	0.2	0.9	0.9	1.5	1.1	(1.7)	1.1	1.2	3.8	1.1	1.1
4000	(1.9)	0.4	0.8	–	1.0	–	0.3	0.3	1.1	(2.3)	1.6	1.1	1.3	1.4	1.2	3.4	1.2	1.0
Approx.	$\approx 0.4 \cdots 1$			≈ 1			≈ 0.3			≈ 1.5			≈ 1			≈ 1 and ≈ 3		
ΔE, ΔQ	±0.03	±0.05	±0.03	±0.02	±0.05	±0.02	±0.02	±0.05	±0.02	±0.03	±0.05	±0.03	±0.03	±0.05	±0.03	±0.02	±0.05	±0.02

Table 2: Apparent diffusion coefficients at given scan rates of a RuO_2/Ti electrode assuming one-electron transfer ($z = 1$) and a real electrode surface of 120 cm^2.

ν (V/s)	4: Ru(III)/(IV) D (cm^2/s)	3: Ru(III)/(IV) D (cm^2/s)	5: Ru(IV)/(V) D (cm^2/s)	6: Ru(V)/(VIII) D (cm^2/s)
Solution	1 M H_2SO_4	1 M NaOH	1 M H_2SO_4	1 M H_2SO_4
0.1	$1.9 \cdot 10^{-15}$	$2.7 \cdot 10^{-15}$	$4.7 \cdot 10^{-15}$	$1.1 \cdot 10^{-14}$
0.2	$3.4 \cdot 10^{-15}$	$5.5 \cdot 10^{-15}$	$9.2 \cdot 10^{-15}$	$2.3 \cdot 10^{-14}$
0.3	$4.5 \cdot 10^{-15}$	$8.9 \cdot 10^{-15}$	$1.2 \cdot 10^{-14}$	$3.0 \cdot 10^{-14}$
1.0	$1.3 \cdot 10^{-14}$	$3.5 \cdot 10^{-14}$	$2.9 \cdot 10^{-14}$	$8.7 \cdot 10^{-14}$
4.0	$5.0 \cdot 10^{-14}$	$1.2 \cdot 10^{-13}$	$1.1 \cdot 10^{-13}$	$2.2 \cdot 10^{-13}$

3.3.2. Peak Currents. At first glance, all peak currents seem to change linearly with scan rate (proportionality $I_p \sim \nu$, Figure 8). Particularly, the fast redox reactions (Peaks 2, 4, 5, and 6) involve adsorbates which cause a more or less constant interface capacitance ($I_p = C\nu$). On the contrary, the hydrogen adsorption reaction in Peak 1 follows $I_p \sim \nu^{1/2}$, which indicates an electrode reaction controlled by diffusion. As well, oxygen diffusion plays a role in the redox reaction Ru(V) → Ru(VIII).

3.3.3. Apparent Diffusion Coefficients. For a reversible reaction, which should be the case for Peaks 4, 5, and 6, the concentration of the active species is related to the peak current. According to the theory of cyclic voltammetry, the diffusion coefficient can be estimated by the help of Randles-Sevčik equation at 25°C [30]:

$$i_p = 2{,}686 \cdot 10^5 z^{3/2} A c^0 D^{1/2} \nu^{1/2}, \quad (14)$$

wherein i_p is peak current (in A), A is electrode cross section (in cm^2), D is diffusion coefficient ($cm^2\ s^{-1} = 10^{-4}\ m^2/s$), c^0 is bulk concentration of the solution ($mol\ cm^{-3} = 1000$ mol/L), and ν is scan rate (V/s).

The apparent diffusion coefficients, compiled in Table 2 and Figure 10, differ from values calculated by the help of molar ion conductivities in infinitely diluted aqueous solution according to the Nernst-Einstein equation, $D = \lambda RT/F^2$ at 25°C.

For the proton, $\lambda(H^+) = 0.03469\ S\ m^2/mol$ corresponds to $D(H^+) = 9.3 \cdot 10^{-5}\ cm^2/s$. For the hydroxide ion, $\lambda(OH^-) = 0.01992\ S\ m^2/mol$ corresponds to $D(OH^-) = 5.3 \cdot 10^{-5}\ cm^2/s$.

The apparent diffusion coefficient per electrode cross section (1 cm^2) rises at high scan rates, that is, $1.9 \cdot 10^{-10}\ cm^2/s$ (at 1 V/s; and $7.1 \cdot 10^{-10}\ cm^2/s$ (4 V/s) for the Ru(III)/Ru(IV) redox couple. With respect to the electrochemically active surface area of 120 cm^2, the diffusion coefficient reads $1.3 \cdot 10^{-14}\ cm^2/s$ at 1 V/s and $5.0 \cdot 10^{-14}\ cm^2/s$ at 4 V/s (Table 2). At low scan rates, the mentioned redox reactions are obviously diffusion controlled in the porous electrode, whereas at fast scan rates the reaction proceeds at the electrode surface and cannot penetrate the pores. It is interesting to note that the calculated electrons for the transition Ru(III)/Ru(IV) drop from $z = 1$ (per Ru atom) at low scan rates to $z = 0.8$ at fast scan rates. The reverse reaction Ru(IV)/Ru(III) yields about 1600 $\mu C/cm^2$, which results in 0.8 ± 0.03 electrons for nearly all scan rates. This again gives a hint at that the electrode reactions take place at the electrode surface at fast scan rates, whereas the total active electrode area can effectively be used at low scan rates only. Fast diffusion process might be attributed to the proton at the surface of the electrode, which is directly coupled with the electronic conductivity: $H_2 \rightarrow 2H^+ + 2e^-$. Zheng et al. proved this proton insertion into ruthenium oxide films prepared by pulsed laser deposition [31].

3.3.4. Oxygen and Hydrogen Evolution. Peak 7 belongs to the oxygen evolution reaction. The pH-dependent OER is usually characterized by the Tafel slopes of the current–voltage characteristics [32]. The mechanism comprises the following: (i) the discharge of water molecules (acid) or OH^- (alkaline) by oxidation at the surface-active sites; (ii) the intermediate OH^* being converted to OH, (iii) the surface complex $M(OH)_2$ being oxidized; and (iv) oxygen being released by the decomposition of two M(OH)O complexes [12].

In acidic solutions, the Tafel slope amounts to 30 mV/dec (1 M H_2SO_4 at 30°C [33]), 42 mV/dec (1 M H_2SO_4 at 20°C) [34], and 30–50 mV/dec in 0.5 M H_2SO_4 at room temperature [35]. The Tafel slope depends on the acid concentration. The quasistationary voltammogram yields 52 mV/dec in 1 M H_2SO_4 (25°C, pH 0.08) above 1.52 V RHE; see Figure 11. The slope is 69.3 ± 0.2 mV/dec (>1.5 V) in 0.1 M H_2SO_4 (pH 1.0) and 35.8 ± 0.1 mV/dec (>1.48 V) in 0.01 M H_2SO_4 (pH 1.71) and below this potential 191.3 ± 1.3 mV/dec. Peak 14 is attributed to the hydrogen evolution reaction (HER). Our results indicate two different slopes: −72.8 ± 0.7 mV/dec at low current densities and −42.3 ± 0.1 mV/dec at high current densities (Figure 12). In 0.1-molar H_2SO_4, the slope was −89.2 ± 0.2 mV/dec at high current densities. In the literature, −60 mV/dec and −40 mV/dec were reported for low and high current densities respectively [12, 36]. The generally accepted mechanism of the hydrogen electrode is of the Volmer-Heyrovsky type:

$$[Ru]\,OH + H^+ + e^- \rightleftharpoons [Ru]\,OH_2 \quad (15)$$

$$[Ru]\,OH_2 + H^+ + e^- \rightleftharpoons [Ru]\,OH + H_2 \quad (16)$$

3.4. Electrochemistry in Alkaline Solution. The reactions of ruthenium oxide electrodes in alkaline solutions were studied by Burke and coworkers in 1980 [37, 38]. In 1-molar NaOH the

OCP of RuO_2 is 0.91 V. We found 13 peaks of interest by using fast scan cyclic voltammetry (Figure 13).

The first two peaks mean 1 (at 52 ± 13 mV) the hydrogen adsorption on coordinatively unsaturated Ru sites and 2 (283 ± 82 mV) the hydrogen adsorption at Ru-O, possibly Ru(II) exists. The corresponding reduction peaks are 11 at 420 ± 67 mV and 12 at ≈ 87 ± 36 mV, respectively. At 639 ± 30 mV, the transition of Ru(III) → Ru(IV) takes place (peak 3) [24, 37, 38].

Peak 4 at approximately 1136 ± 19 mV reflects the Ru(IV) → Ru(VI) transition. Ru(V) is not likely to appear in alkaline solutions although it might be an intermediate during the formation of Ru(VI). Ru(VI) is known as ruthenate (RuO_4^{2-}) in alkaline solutions [24, 27, 29].

$$\text{Peak } 4\text{: } RuO_4^{2-} + 4H^+ + 2e^- \rightleftharpoons RuO_2 + 2H_2O \quad (17)$$

Peak 4 corresponds to the reduction peak 9 at 1060 ± 21 mV. This was confirmed by examinations using benzaldehyde and benzyl alcohol. Ru(VI) is able to oxidize benzaldehyde but not benzyl alcohol. Ru(VII) oxidizes both [24]. At about 1392 ± 14 mV, the striking peak 5 arises, and the reduction peak 8 at approximately 1368 ± 5 mV. This highly reversible redox reaction reflects Ru(VI) → Ru(VII).

$$\text{Peak } 5\text{: } RuO_4^- + e^- \rightleftharpoons RuO_4^{2-} \quad (18)$$

Peak 5 appears only in strongly alkaline solutions. Burke et al. mention a potential range within 1.35–1.45 V. This peak does not depend on pH, but the hydroxide concentration of the solution plays a role [24, 37, 38]. The existence of perruthenate (RuO_4^-) was proved by in situ IR spectroscopy [29].

A further increase in potential leads to the oxygen evolution reaction, peak 6 at about 1462 ± 34 mV. During the OER, further transition to Ru(VIII) might take place. However, Ru(VIII) is not stable in alkaline solutions [27, 29].

$$\text{Peak } 6\text{: } HRuO_5^- + H^+ + e^- \rightleftharpoons RuO_4^- + H_2O \quad (19)$$

3.4.1. Electrochemical Valency. Based on the Ru(III)/Ru(IV) redox couple, which requires an electric charge of approximately 2000 $\mu C/cm^2$ for $z = 1$ transferred electron (per Ru atom), the values in Table 3 were calculated. It is interesting to note that the calculated electrons for Peak 1 in alkaline solution differ from those in acidic solutions. There is evidence for a one-electron transfer, but the peak current ratio suggests a highly irreversible electron transfer. We conclude that Peak 1 is the hydrogen adsorption reaction on the coordinatively unsaturated Ru atom. The calculated electrons at Peak 2 are most surprising in the range between 1.1 and 2.8. This might be a hint at the formation Ru(II) in alkaline solutions; possibly a surface species "$Ru(OH)_2$" is able to directly bind hydroxyl ions. The peak current ratios give evidence for a reversible electron transfer, especially at fast scan rates.

The conversion of Ru(III) to Ru(IV) is known to be a highly reversible reaction. The difference of the peak potential indicates a one-electron transfer reaction as has been assumed by many authors [3]. The charge calculations give hints that $z \approx 1.5$ electrons (or protons or rather hydroxide ions) are involved per Ru atom. Burke and Healy [24] suggested therefore the following reaction:

$$RuO_2 + 2{,}5OH^- \rightleftharpoons RuO_2(OH)_{2,5}^{0,5-} + 2e^- \quad (20)$$

Regardless of whether 2 mC/cm^2 is consumed by one, 1.5, or two electrons, the peak current ratio shows a high reversibility. Closer examination of the Ru(IV)/Ru(III) peak 10 shows a two-electron transfer reaction at low scan rates, and a one-electron transfer at high scan rates. It is striking that the calculated electrons give exactly $z = 2$ (<300 mV/s), $z = 1.5$ at 300 mV/s, and $z = 1$ (>300 mV/s). Obviously, a slow and a fast step is involved in the Ru(III)/Ru(IV) transition.

As expected peak 5, the Ru(IV) → Ru(VI) reaction, involves 2 electrons and shows high reversibility.

Peak 6 is the transition of Ru(VI) → Ru(VII). Higher oxides are more stable in alkaline solution than in acids, and this peak only appears at this alkaline pH [39].

Chu et al. [4] demonstrated the presence of two types of water monolayers having different densities at the RuO_2(110)–water interface in 0.1 M NaOH. At potentials close to the OER, external water molecules and surface hydroxide form a bilayer with O-H-O bond distances similar to that of ice (Figure 14).

The oxygen evolution 6 is followed by the reduction peak 7. This shoulder in the voltammogram is caused by the Ru(VIII) → Ru(VII) transition. Thermodynamic calculations for (19) result in the potential $E^0 = 1.678$ V (11.53 < pH < 14.00), so that this transition most likely takes place during the OER.

3.4.2. Peak Currents. With respect to the correlation between peak current and scan rate (Figure 15), peak 1 could not be evaluated correctly at fast scan rates due to overlap with peak 2. In alkaline solution, the so-called hydrogen adsorption might result from the high hydroxide concentration rather than from hydrogen or hydronium ions. Peak 2 shows $I_p \sim \nu^{1/2}$ at fast scan rates (>500 mV/s) and $I_p \sim \nu$ at low speed.

The similar properties of Peak 2 and Peak 3 might indicate a more or less stable species in alkaline solutions, that is, Ru(II) or a mixed species of Ru(I) and Ru(III). We propose these species based on the calculated number of transferred electrons (Table 3). Ru(II) is known in complexes, especially such containing chloride ligands. Mercer and Buckley [40] characterized hexaaquaruthenium(II) $[Ru(H_2O)_6]^{2+}$ in aqueous solution by electrolytic reduction of Ru(III). The oxidation state was verified by coulometry and titration with triiodide, which might be a coincidence, the potential of peak 2 in acidic solution (143 ± 9 mV) is half that in alkaline solution (283 ± 82 mV), where Ru(II) forms stable hydroxospecies in contrast to a cluster ion in acids. Peak 4 and Peak 5 obey roughly $I_p \sim \nu$. Peak 5 involves the adsorption of external water molecules.

3.4.3. Apparent Diffusion Coefficient. According to Randles-Sevčik equation at 25°C, the apparent diffusion coefficients are compiled in Figure 16. The redox couples Ru(II)/Ru(III) and Ru(VI)/Ru(VII) behave similarly during the oxidation.

Table 3: Calculated electrons for each redox reaction using peak potential differences and calculated charges at different scan rates in 1 M NaOH. For details, compare with Table 1.

Peak	1: Ru-H			2: possibly Ru(II)/Ru(III)			3: $Ru_2(III)O_3/2Ru(IV)O_2$			10	4: Ru(IV) → Ru(VI)			5: Ru(VI)\Ru(VII)			8
mV/s	$z(\Delta E_p)$	$z(Q)$	$i_p{}^a/i_p{}^c$	$z(\Delta E_p)$	$z(Q)$	$i_p{}^a/i_p{}^c$	$z(\Delta E_p)$	$z(Q)$	$i_p{}^a/i_p{}^c$	$z(Q)$	$z(\Delta E_p)$	$z(Q)$	$i_p{}^a/i_p{}^c$	$z(\Delta E_p)$	$z(Q)$	$i_p{}^a/i_p{}^c$	$z(Q)$
100	1.3	1.0	0.4	(5.8)	2.0	0.4	0.7	2.0	0.6	2.0	(19)	2.0	0.5	(7.4)	1.0	0.5	(3.0)
200	(6.1)	0.4	0.5	0.2	1.1	0.5	0.8	2.7	0.8	2.0	1.2	2.4	1.0	(7.3)	1.1	0.8	(3.0)
300	(4.5)	0.4	0.5	0.2	1.2	0.6	0.7	2.8	1.0	1.4	0.6	2.3	1.2	(4.7)	1.4	0.9	2.2
500	(2.8)	0.8	0.6	0.2	2.7	0.8	0.5	2.5	1.2	1.0	1.0	2.5	1.4	(4.0)	2.0	1.0	2.0
1000	-	0.9	-	0.4	2.8	1.0	0.7	2.3	1.5	1.0	0.5	2.4	1.7	(3.0)	2.0	1.1	2.0
2000	-	1.0	-	0.9	2.4	1.0	0.6	2.3	1.7	1.0	0.7	2.5	1.7	2.2	2.0	1.2	2.0
3000	-	1.0	-	(5.8)	2.5	1.0	0.7	1.9	1.6	1.1	0.7	2.5	1.7	1.1	2.0	1.0	2.1
4000	-	1.0	-	1.7	2.5	0.9	0.5	1.5	1.7	1.1	0.5	2.4	1.7	1.1	2.1	1.2	2.2
Approx.		≈1			≈1 ⋯ 2.5			≈0.8 ⋯ 2		≈1		≈0.8 and ≈2			≈1 ⋯ 2		≈2
ΔE, ΔQ	±0.04	±0.05	±0.04	±0.15	±0.05	±0.15	±0.04	±0.05	±0.04	±0.05	±0.03	±0.05	±0.03	±0.02	±0.05	±0.02	±0.02

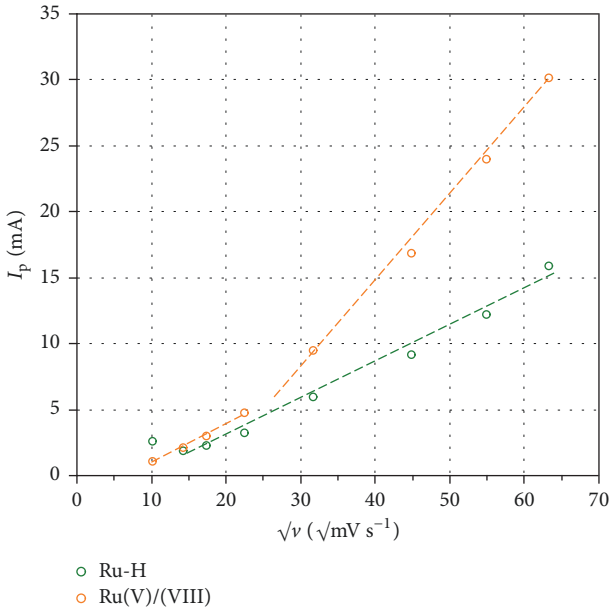

FIGURE 9: Changes of peak current against the square root of scan rate in order to identify diffusion and adsorption controlled electrochemical processes. Fit quality: Ru-H ($R^2 = 0.989$; 0.2–4 V/s); Ru(V)/(VIII) ($R^2 = 0.995$; 0.1–0.5 V/s; $R^2 = 0.996$; >1.0 V/s).

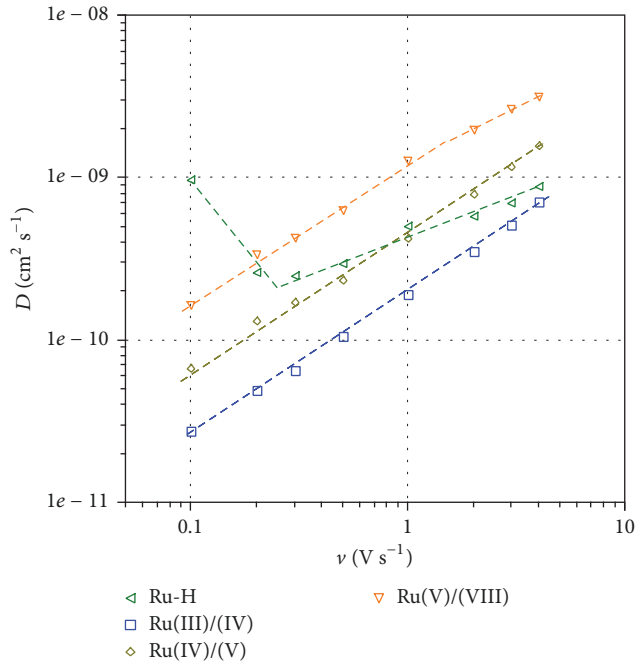

FIGURE 10: Apparent diffusion coefficients at different scan rates according to Randles-Sevčik equation for a RuO_2/Ti electrode in 1-molar H_2SO_4 at 25°C assuming one-electron transfer ($z = 1$) and unit surface area (1 cm^2) for reason of comparability. Fit quality: Ru-H ($R^2 = 0.9511$, >0.3 V/s); Ru(III)/(IV) ($R^2 = 0.9952$); Ru(IV)/(V) ($R^2 = 0.9995$); Ru(V)/(VIII) ($R^2 = 0.997$; 0.1–1 V/s) and ($R^2 = 0.991$; >1 V/s).

The diffusion coefficients of Ru(III)/Ru(IV) and vice versa behave differently, so that the apparent diffusion coefficient is higher in alkaline solution than in acid solution; see Table 2. This can be explained by a stronger oxide growth in alkaline solution due to the formation of more permeable and crystalline deposits [39].

3.4.4. Oxygen and Hydrogen Evolution. The oxygen evolution reaction [23, 41–43] in 1 M NaOH can be divided into two regions. The Tafel slope amounts to (i) 93 mV/dec below 1.5 V and (ii) 42 mV/dec above 1.5 V; see Figure 11. Two different slopes were also observed during the hydrogen evolution reaction in 1 M NaOH. In the literature, 30–60 mV/dec and 120 mV/dec can be found for steady-state measurements [12]. Two different slopes were also observed for the hydrogen evolution reaction: (i) 40–50 mV/dec at low current densities and (ii) 230–240 mV/dec at high current densities [12]. The different slopes suggest a change in the reaction regime depending on current [12].

4. Conclusion and Outlook

This paper gives a comprehensive overview on the redox electrochemistry and voltammetric behavior of ruthenium dioxide, which cannot be found in detail in the literature. For the first time, all the 13 voltammetric peaks were assigned to a consistent set of electrode reactions both in acid and in alkaline solution. A most illustrative mechanism for the dissociative adsorption of water that causes the redox activity of RuO_2 is given in Figure 5.

(1) Under fast scan rates up to 4000 mV/s, 13 peaks were identified in acidic and in alkaline solution, which reflect the high reversibility of RuO_2. The underlying electrode reactions were compiled for each peak with respect to the more recent literature and our own observations. The peak current I of most peaks, especially the Ru(III)/Ru(IV) transition, increases with rising scan rate v which is due to the capacitive properties of the metal oxide surface ($I = Cv$). Diffusion controlled processes that cause a nonlinear function $I \sim v^{1/2}$ were observed for the hydrogen sorption.

(2) Below 0.4 V RHE, in the "hydrogen adsorption region," the dissociate adsorption of water takes place, whereby Ru-OH species are formed. In the hydrogen region, Ru(II) or a mixed species Ru(I)−Ru(III) is likely to be present, which we proved by the help of voltammetric charge. In alkaline solution, the aqua complex $[Ru(H_2O)_6]^{2+}$ seems reasonable (283 ± 82 mV) according to our results, whereas in the solid material a mixed-valent hydroxospecies is likely to be.

(3) Above 0.4 V RHE the ruthenium surface passes through the oxidation states III → IV → V → VIII in acids and III → IV → VI → VII → (VIII) in alkaline solution. We found that the electrochemical valency is different in alkaline and acidic solution; therefore, the redox processes cannot be written with general equations for any pH value.

(4) The Ru(III)/Ru(IV) couple is involved in a one-electron electron transfer (per Ru atom). Hints at $z \approx 1.5$ suggest complex cluster species. Simplifying, we propose a

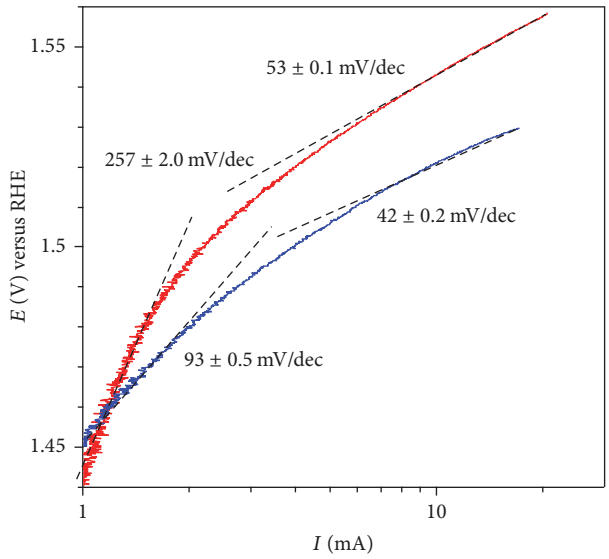

Figure 11: Oxygen evolution at a Ti/RuO_2 electrode in 1 M H_2SO_4 (red line) and 1 M NaOH (blue line) at 25°C derived from cyclic voltammogram (oxidation sweep at 100 mV/s).

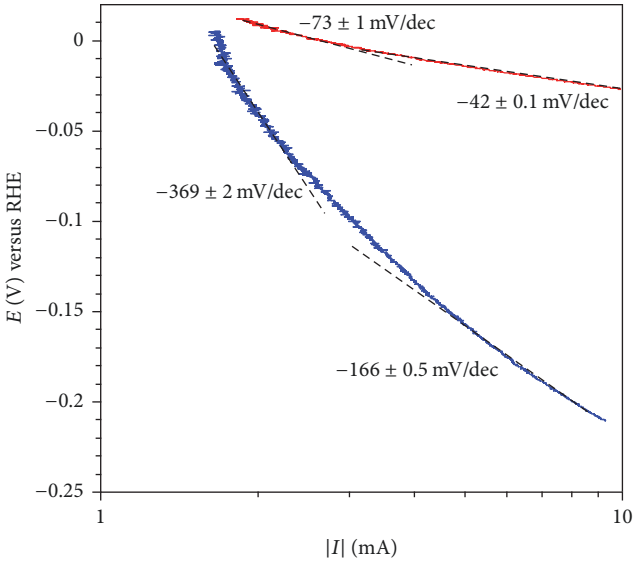

Figure 12: Hydrogen evolution at a Ti/RuO_2 electrode in 1 M H_2SO_4 (red line) and 1 M NaOH (blue line) at 25°C derived from cyclic voltammogram (reduction sweep at 100 mV/s).

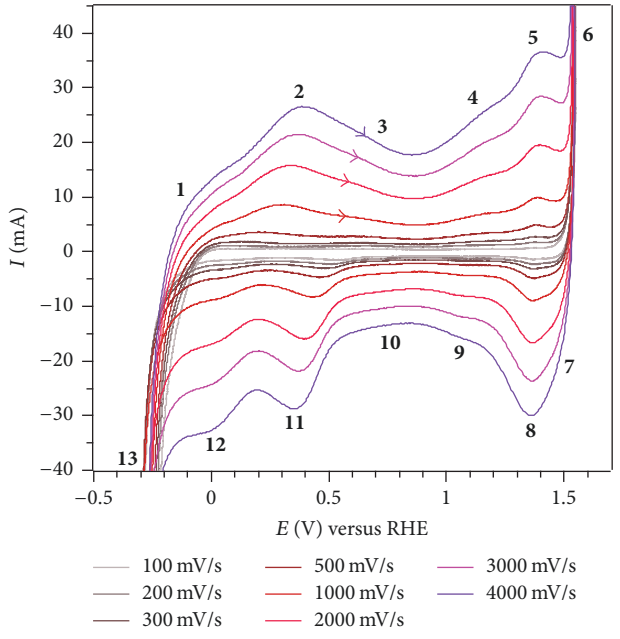

Figure 13: Cyclic voltammograms of a RuO_2/Ti electrode in 1 M NaOH (pH 12.93) at different scan rates. Reference: reversible hydrogen electrode. The electrolyte resistance was corrected (R_e = 2.8 Ω). Arrows: oxidation wave in anodic direction.

species $Ru(OH)_3 \cdot RuO_2$ that is present at the electrode surface and explains the oxygen surplus found in the EDX analysis.

(5) The diffusion coefficients according to Randles-Sevčik equation allow distinguishing pore diffusion at low scan rates from rapid surface diffusion of adsorbates at fast scans. On the other hand, these values show that diffusion coefficients deduced by CV peaks must be treated with caution, especially at high scan rates. RuO_2 is known for its high pseudocapacitance [13], $C = dQ/dE$, which results from large potential gradients across the oxide-electrolyte interface. Therefore, we suggest evaluating the *inflexion points* in Figures 9 and 15 with respect to a change of mass transport. At low scan rates, diffusion is able to penetrate into the depth of the porous material, whereas fast scan rates just allow double-layer charging at the electrode surface. We conclude that the proton is fast enough to take part in the redox reaction Ru(III)/Ru(IV), even above 1000 mV/s without significant limitation by diffusion. Once adsorbed hydrogen or oxygen

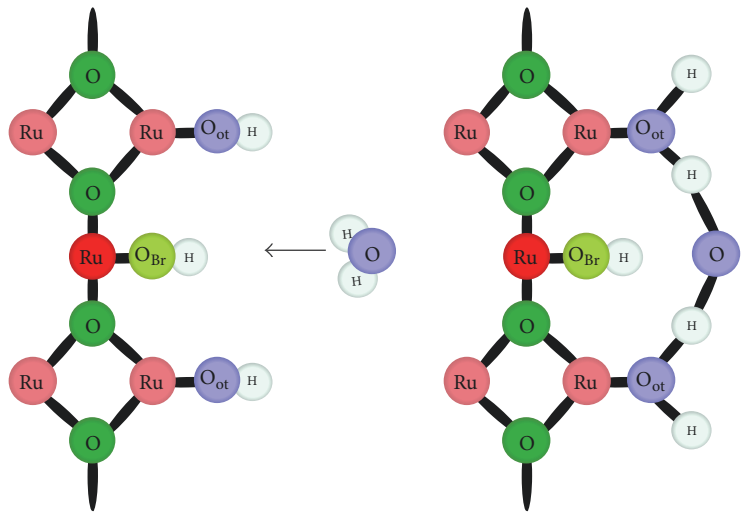

FIGURE 14: Formation of double layer similar to ice from external water molecule adsorption at 1.39 V on hydroxyl groups (modified after [4]).

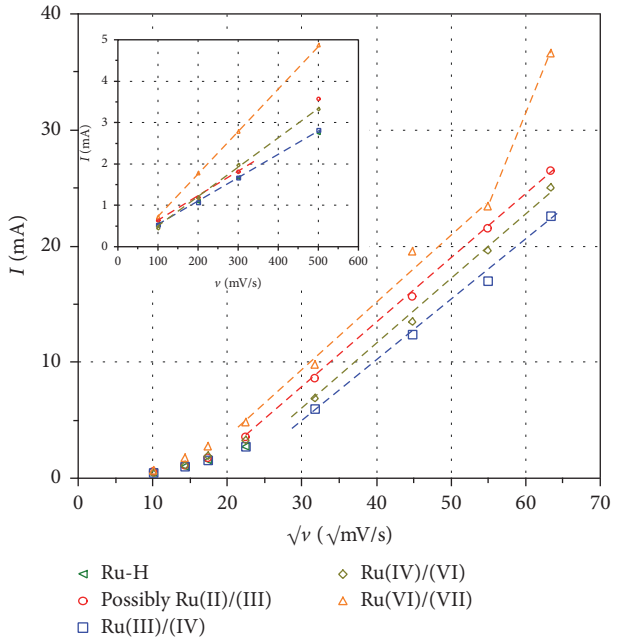

FIGURE 15: Voltammetric peak currents against the square root of scan rate: RuO_2/Ti electrode in 1 M NaOH; Insert: peak current versus scan rate. Fit quality for $I_p \sim \nu$ (0.1–0.5 V/s): Ru-H (R^2 = 0.9999); possibly Ru(II)/(III) (R^2 = 0.988); Ru(III)/(IV) (R^2 = 0.9998); Ru(IV)/(VI) (R^2 = 0.9991); Ru(VI)/(VII) (R^2 = 1); fit quality for $I_p \sim \nu^{1/2}$ (>1.0 V/s): possibly Ru(II)/(III) (R^2 = 0.9996); Ru(III)/(IV) (R^2 = 0.994); Ru(IV)/(VI) (R^2 = 0.996); Ru(VI)/(VII) (R^2 = 0.939).

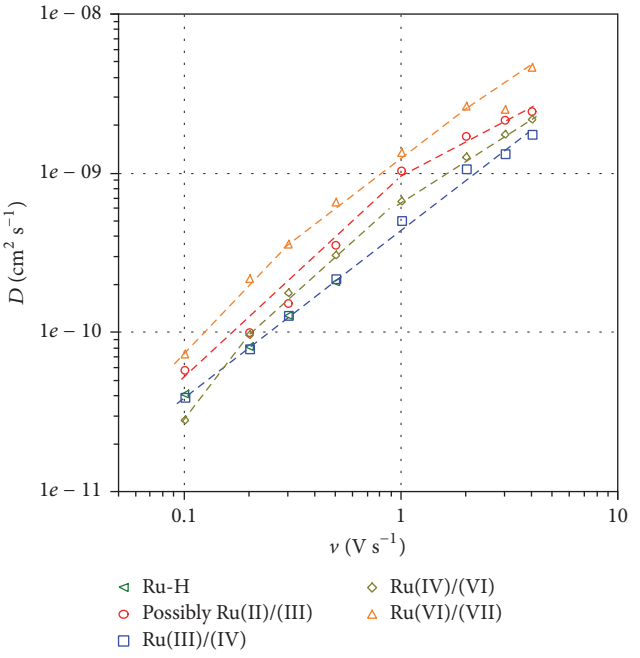

FIGURE 16: Apparent diffusion coefficients at different scan rates: RuO_2/Ti electrode in 1 M NaOH at 25°C assuming one-electron transfer (z = 1) and unit surface area (1 cm^2) for reason of comparability. Fit quality: Ru-H (R^2 = 0.9996; 0.1–0.4 V/s); possibly Ru(II)/(III) (R^2 = 0.961; 0.1–0.5 V/s) and (R^2 = 0.965; >0.5 V/s); Ru(III)/(IV) (R^2 = 0.991); Ru(IV)/(VI) (R^2 = 0.998; 0.1–0.5 V/s) and (R^2 = 0.993; >1.0 V/s); Ru(VI)/(VII) (R^2 = 0.9998; 0.1–0.3 V/s) and (R^2 = 0.932, >0.3 V/s).

species are involved, the slope dD/dν gets smaller, and the inflexion point lies at a far lower scan rate. Summarizing, a constant diffusion coefficient was not found even in the volt-per-second range.

Conflicts of Interest

The authors declare that they have no conflicts of interest.

Acknowledgments

This work was financially supported by the Bavarian State Ministry of the Environment and Consumer Protection.

References

[1] P. Kurzweil, "Metal oxides and ion-exchanging surfaces as pH sensors in liquids: state-of-the-art and outlook," *Sensors*, vol. 9, no. 6, pp. 4955–4985, 2009.

[2] Y. Takasu, W. Sugimoto, Y. Nishiki, and S. Nakamatsu, "Structural analyses of RuO_2-TiO_2/Ti and IrO_2-RuO_2-TiO_2/Ti anodes used in industrial chlor-alkali membrane processes," *Journal of Applied Electrochemistry*, vol. 40, no. 10, pp. 1789–1795, 2010.

[3] K. Doblhofer, M. Metikos, Z. Ogumi, and H. Gerischer, "Electrochemical oxidation and reduction of the RuO_2/Ti electrode surface," *Berichte der Bunsen-Gesellschaft: Physical Chemistry, Chemical Physics*, vol. 82, no. 10, pp. 1046–1050, 1978.

[4] Y. S. Chu, T. E. Lister, W. G. Cullen, H. You, and Z. Nagy, "Commensurate water monolayer at the RuO_2 (110)/water interface," *Physical Review Letters*, vol. 86, no. 15, pp. 3364–3367, 2001.

[5] S. Trasatti and G. Buzzanca, "Ruthenium dioxide: A new interesting electrode material. Solid state structure and electrochemical behaviour," *Journal of Electroanalytical Chemistry*, vol. 29, no. 2, pp. A1–A5, 1971.

[6] D. O. Wipf, E. W. Kristensen, M. R. Deakin, and R. M. Wightman, "Fast-Scan cyclic voltammetry as a method to measure rapid, heterogenous electron-transfer kinetics," *Analytical Chemistry*, vol. 60, no. 4, pp. 306–310, 1988.

[7] C. E. John and S. R. Jones, *Fast Scan Cyclic Voltammetry of Dopamine and Serotonin in Mouse Brain Slices, Electrochemical Methods for Neuroscience*, CRC Press/Taylor and Francis, Boca Raton, FL, USA, 2007.

[8] A. E. Newkirk and D. W. McKee, "Thermal decomposition of rhodium, iridium, and ruthenium chlorides," *Journal of Catalysis*, vol. 11, no. 4, pp. 370–377, 1968.

[9] R. F. Savinell, R. L. Zeller, and J. A. Adams, "Electrochemically active surface area: voltammetric charge correlations for ruthenium and iridium dioxide electrodes," *Journal of The Electrochemical Society*, vol. 137, no. 2, pp. 489–494, 1990.

[10] T. Hepel, F. H. Pollak, and W. E. O'Grady, "Effect of crystallographic orientation of single-crystal ru_2 electrodes on the hydrogen adsorption reactions," *Journal of The Electrochemical Society*, vol. 131, no. 9, pp. 2094–2100, 1984.

[11] H. J. Zhang, B. Lu, H. Y. Li, S. N. Bao, and P. He, "Scanning tunneling microscopy and ultraviolet photoemission spectroscopy studies of oxygen adsorption on Ru(1010)," *Surface Science*, vol. 556, no. 1, pp. 63–68, 2004.

[12] H. Over, "Surface chemistry of ruthenium dioxide in heterogeneous catalysis and electrocatalysis: From fundamental to applied research," *Chemical Reviews*, vol. 112, no. 6, pp. 3356–3426, 2012.

[13] P. Kurzweil, "Precious metal oxides for electrochemical energy converters: pseudocapacitance and pH dependence of redox processes," *Journal of Power Sources*, vol. 190, no. 1, pp. 189–200, 2009.

[14] H. Over, A. P. Seitsonen, E. Lundgren, M. Schmid, and P. Varga, "Experimental and simulated STM images of stoichiometric and partially reduced RuO_2(110) surfaces including adsorbates," *Surface Science*, vol. 515, no. 1, pp. 143–156, 2002.

[15] H. Over and A. P. Seitsonen, "Surface chemistry: Oxidation of metal surfaces," *Science*, vol. 297, no. 5589, pp. 2003–2005, 2002.

[16] M. Todorova, W. X. Li, M. V. Ganduglia-Pirovano, C. Stampfl, K. Reuter, and M. Scheffler, "Role of subsurface oxygen in oxide formation at transition metal surfaces," *Physical Review Letters*, vol. 89, no. 9, Article ID 096103, pp. 961031–961034, 2002.

[17] D. Galizzioli, F. Tantardini, and S. Trasatti, "Ruthenium dioxide: a new electrode material. I. Behaviour in acid solutions of inert electrolytes," *Journal of Applied Electrochemistry*, vol. 4, no. 1, pp. 57–67, 1974.

[18] S. Hadži-Jordanov, H. Angerstein-Kozlowska, and B. E. Conway, "Surface oxidation and H deposition at ruthenium electrodes: Resolution of component processes in potential-sweep experiments," *Journal of Electroanalytical Chemistry*, vol. 60, no. 3, pp. 359–362, 1975.

[19] D. Michell, D. A. J. Rand, and R. Woods, "A study of ruthenium electrodes by cyclic voltammetry and X-ray emission spectroscopy," *Journal of Electroanalytical Chemistry*, vol. 89, no. 1, pp. 11–27, 1978.

[20] R. Koncki and M. Mascini, "Screen-printed ruthenium dioxide electrodes for pH measurements," *Analytica Chimica Acta*, vol. 351, no. 1-3, pp. 143–149, 1997.

[21] L. Manjakkal, K. Zaraska, K. Cvejin, J. Kulawik, and D. Szwagierczak, "Potentiometric RuO2-Ta2O5 pH sensors fabricated using thick film and LTCC technologies," *Talanta*, vol. 147, pp. 233–240, 2016.

[22] D. Galizzioli, F. Tantardini, and S. Trasatti, "Ruthenium dioxide: a new electrode material. II. Non-stoichiometry and energetics of electrode reactions in acid solutions," *Journal of Applied Electrochemistry*, vol. 5, no. 3, pp. 203–214, 1975.

[23] L. D. Burke, O. J. Murphy, J. F. O'Neill, and S. Venkatesan, "The oxygen electrode. Part 8. - Oxygen evolution at ruthenium dioxide anodes," *Journal of the Chemical Society, Faraday Transactions 1: Physical Chemistry in Condensed Phases*, vol. 73, pp. 1659–1671, 1977.

[24] L. D. Burke and J. F. Healy, "The importance of reactive surface groups with regard to the electrocatalytic behaviour of oxide (especially RuO_2) anodes," *Journal of Electroanalytical Chemistry*, vol. 124, no. 1-2, pp. 327–332, 1981.

[25] E. J. M. O'Sullivan and E. J. Calvo, "Chapter 3 reactions at metal oxide electrodes," *Comprehensive Chemical Kinetics*, vol. 27, pp. 247–360, 1988.

[26] R. Kötz, H. J. Lewerenz, and S. Stucki, "XPS studies of oxygen evolution on Ru and RuO_2 Anodes," *Journal of The Electrochemical Society*, vol. 130, no. 4, pp. 825–829, 1983.

[27] I. Povar and O. Spinu, "Ruthenium redox equilibria: 3. Pourbaix diagrams for the systems Ru-H_2O and Ru-Cl^--H_2O," *Journal of Electrochemical Science and Engineering*, vol. 6, no. 1, pp. 145–153, 2016.

[28] R. Kötz, S. Stucki, D. Scherson, and D. M. Kolb, "In-situ identification of RuO_4 as the corrosion product during oxygen evolution on ruthenium in acid media," *Journal of Electroanalytical Chemistry*, vol. 172, no. 1-2, pp. 211–219, 1984.

[29] A. Bewick, C. Gutiérrez, and G. Larramona, "In-situ IR spectroscopy study of the ruthenium electrode in acid and alkaline solutions," *Journal of Electroanalytical Chemistry*, vol. 332, no. 1-2, pp. 155–167, 1992.

[30] M. Barbooti, *Environmental Applications of Instrumental Chemical Analysis*, Apple Academic Press, 2015.

[31] J. P. Zheng, T. R. Jow, Q. X. Jia, and X. D. Wu, "Proton insertion into ruthenium oxide film prepared by pulsed laser deposition,"

Journal of The Electrochemical Society, vol. 143, no. 3, pp. 1068–1070, 1996.

[32] K. A. Stoerzinger, R. R. Rao, X. R. Wang, W. T. Hong, C. M. Rouleau, and Y. Shao-Horn, "The Role of Ru Redox in pH-Dependent oxygen evolution on rutile ruthenium dioxide surfaces," *Chemistry of Materials*, vol. 2, no. 5, pp. 668–675, 2017.

[33] C. Iwakura, K. Hirao, and H. Tamura, "Anodic evolution of oxygen on ruthenium in acidic solutions," *Electrochimica Acta*, vol. 22, no. 4, pp. 329–334, 1977.

[34] E. Fabbri, A. Habereder, K. Waltar, R. Kötz, and T. J. Schmidt, "Developments and perspectives of oxide-based catalysts for the oxygen evolution reaction," *Catalysis Science and Technology*, vol. 4, no. 11, pp. 3800–3821, 2014.

[35] M. Vuković, "Oxygen evolution on an electrodeposited ruthenium electrode in acid solution -the effect of thermal treatment," *Electrochimica Acta*, vol. 34, no. 2, pp. 287–291, 1989.

[36] E. R. Kötz and S. Stucki, "Ruthenium dioxide as a hydrogen-evolving cathode," *Journal of Applied Electrochemistry*, vol. 17, no. 6, pp. 1190–1197, 1987.

[37] L. D. Burke and O. J. Murphy, "The electrochemical behaviour of RuO_2-based mixed-oxide anodes in base," *Journal of Electroanalytical Chemistry*, vol. 109, no. 1-3, pp. 199–212, 1980.

[38] L. D. Burke and D. P. Whelan, "The behaviour of ruthenium anodes in base," *Journal of Electroanalytical Chemistry*, vol. 103, no. 2, pp. 179–187, 1979.

[39] L. D. Burke, J. K. Mulcahy, and S. Venkatesan, "An investigation of anodic film formation on electrodeposited ruthenium by potential sweep techniques," *Journal of Electroanalytical Chemistry*, vol. 81, no. 2, pp. 339–346, 1977.

[40] E. E. Mercer and R. R. Buckley, "Hexaaquoruthenium(II)," *Inorganic Chemistry*, vol. 4, no. 12, pp. 1692–1695, 1965.

[41] T. Reier, M. Oezaslan, and P. Strasser, "Electrocatalytic oxygen evolution reaction (OER) on Ru, Ir, and pt catalysts: a comparative study of nanoparticles and bulk materials," *ACS Catalysis*, vol. 2, no. 8, pp. 1765–1772, 2012.

[42] M. H. Miles, E. A. Klaus, B. P. Gunn, J. R. Locker, W. E. Serafin, and S. Srinivasan, "The oxygen evolution reaction on platinum, iridium, ruthenium and their alloys at 80°C in acid solutions," *Electrochimica Acta*, vol. 23, no. 6, pp. 521–526, 1978.

[43] Y. Lee, J. Suntivich, K. J. May, E. E. Perry, and Y. Shao-Horn, "Synthesis and activities of rutile IrO_2 and RuO_2 nanoparticles for oxygen evolution in acid and alkaline solutions," *The Journal of Physical Chemistry Letters*, vol. 3, no. 3, pp. 399–404, 2012.